Dalton Transactions

Accepted Manuscript

ROYAL SOCIETY OF CHEMISTRY

www.rsc.org/dalton

Journal Name

RSCPublishing

ARTICLE

Bright Luminescence in Lanthanide Coordination Polymers with Tetrafluoroterephthalate as a Bridging Ligand

Cite this: DOI: 10.1039/xoxxoooooox

Received ooth January 2012,
Accepted ooth January 2012

DOI: 10.1039/xoxxoooooox

www.rsc.org/

Miriam Sobieray,[a] Jens Gode,[a] Christiane Seidel,[a] Marieke Poß,[b] Claus Feldmann,[b] Uwe Ruschewitz*[a]

Ten new coordination polymers of the general compositions $^{2}_{\infty}$[Ln^{III}(tfBDC)(NO_3)($DMF)_2$]·DMF with Ln^{III} = Eu^{3+} (**1**), Gd^{3+} (**2**), Tb^{3+} (**3**), Ho^{3+} (**4**), Tm^{3+} (**5**), $^{2}_{\infty}$[Ln^{III}(tfBDC)(CH_3COO)($FA)_3$]·3FA with Ln^{III} = Sm^{3+} (**6**), Eu^{3+} (**7**) and $^{2}_{\infty}$[Ln^{III}(tfBDC)(NO_3)($DMSO)_2$] with Ln^{III} = Ho^{3+} (**8**), Er^{3+} (**9**) and Tm^{3+} (**10**) were synthesized and structurally characterized by X-ray single crystal diffraction ($tfBDC^{2-}$ = 2,3,5,6-tetrafluoroterephthalate, DMF = N,N'-dimethylformamide, FA = formamide, DMSO = dimethyl sulfoxide). **1** – **5** crystallize in the monoclinic space group *C*2/*c* with *Z* = 8, **6** and **7** in $P\bar{1}$ with *Z* = 2 and **8** – **10** in *Pbca* with *Z* = 8. All crystal structures contain binuclear lanthanide nodes that are connected by 2,3,5,6-tetrafluoroterephthalates ($tfBDC^{2-}$) to form two-dimensional polymeric structural units. Despite this common structural feature the coordination within these binuclear units is quite different in detail, e.g. CN = 9 for **1** - **7** and CN = 8 for **8** – **10**. The emission spectra of the Europium (**1**, **7**) and Terbium (**3**) compounds reveal intense red and green emission in the visible. The resulting high quantum yields of 53 % (**1**) and 67 % (**3**) at room temperature show that the replacement of organic ligands with C-H groups by perfluorinated ligands leads to compounds with intense emission, as vibrational quenching is reduced. On the other hand, the influence of the coordinating solvent and additional ligands cannot be neglected, as the replacement of DMF by FA and NO_3^- by CH_3COO^- in **7** leads to a reduced quantum yield of only 10 %. Thermoanalytical investigations show that all compounds are stable up to 100 – 150 °C, before a stepwise release of solvent molecules starts followed by a decomposition of the coordination polymer.

Introduction

Coordination polymers (CPs) and metal organic frameworks (MOFs) have been investigated by many research groups world-wide during the last 15 years. With respect to applications most of this work has been focused on the porosity of some of these compounds.

But it has already been emphasized that "the field has other opportunities to offer."[1] Therefore a clear trend can be identified in the field of coordination polymers in the last years, i.e. target-oriented synthesis of new ligands for the construction of CPs with new properties and functionalities. In this respect the synthesis of CPs with fluorinated or perfluorinated linkers has attracted an increasing attention, as these compounds are supposed to show enhanced adsorption properties[2-6] as well as improved luminescence[7] compared to CPs with typical organic ligands. The latter is due to the fact that C-H quenching, which typically reduces the luminescence in organic compounds, is not possible in perfluorinated organics. A linker commonly used in the construction of such coordination polymers is perfluorinated terephthalate.[8] Based on an improved synthesis of this linker, which allows to synthesize gram quantities of tetrafluoroterephthalic acid in high purity starting from cheaply available chemicals,[9] we have synthesized several coordination polymers with perfluorinated terephthalate as linker.[10-11] We mainly focused on the luminescence properties of these compounds and showed that coordination polymers of general composition $^{2}_{\infty}$[Ln^{III}(tfBDC)(NO_3)($DMF)_2$]·DMF (Ln^{3+} = Ce, Pr, Nd, Sm, Dy, Er, Yb; DMF = *N*,*N'*-dimethylformamide) gave intense emissions in the visible region of light for Pr, Sm and Dy with colors ranging from orange, orange-red to warm white.[11] Their crystal structures consist of binuclear lanthanide nodes (CN = 9) connected by 2,3,5,6-tetrafluoroterephthalates ($tfBDC^{2-}$) to form two-dimensional polymeric structural units. DMF as well as NO_3^- are also included in the first coordination sphere of the lanthanides. The latter seems to be important for the rigidity of the polymer. In similar compounds of composition $^{2}_{\infty}$[(Ln^{III})$_2$($tfBDC)_3$($DEF)_2$($EtOH)_2$]·2DEF (Ln^{III} = Tb, Gd, Eu, La, Nd; DEF = *N*,*N'*-diethylformamide),[12] which also consist of binuclear lanthanide nodes connected by $tfBDC^{2-}$ ligands to form 2D sheets, no additional anions like nitrates are included in the first coordination sphere of the lanthanide. Red and green emissions have been reported for the Eu(III) and Tb(III) compounds.[12] In the following we will present our results on

coordination polymers of composition $^{2}_{\infty}$ [Ln^{III}(tfBDC)(NO_3)($DMF)_2$]·DMF with Ln^{III} = Eu^{3+} (**1**), Gd^{3+} (**2**), Tb^{3+} (**3**), Ho^{3+} (**4**) and Tm^{3+} (**5**). They are isostructural to the already reported compounds[11] thus completing this series of compounds for all lanthanides with the exception of La^{3+}, Pm^{3+} and Lu^{3+}. As expected red (Eu^{3+}) and green (Tb^{3+}) emissions are found, but high quantum yields of up to 53 % for the Eu^{3+} and 67 % for the Tb^{3+} compound are remarkable. To investigate the influence of the incorporated DMF molecules and NO_3^- anions on their luminescent properties crystallization from other solvents with other starting materials (Ln(III) acetates instead of Ln(III) nitrates) was attempted. Thus, five new coordination polymers of composition $^{2}_{\infty}$ [Ln^{III}(tfBDC)(CH_3COO)($FA)_3$]·3FA with Ln^{III} = Sm^{3+} (**6**), Eu^{3+} (**7**) and $^{2}_{\infty}$ [Ln^{III}(tfBDC)(NO_3)($DMSO)_2$] with Ln^{III} = Ho^{3+} (**8**), Er^{3+} (**9**) and Tm^{3+} (**10**) were obtained (FA = formamide, DMSO = dimethyl sulfoxide).

Results and discussion

By a diffusion controlled crystallization method developed earlier[11] (see experimental section) we were able to synthesize single crystals with sizes up to several millimeters of coordination polymers with the general formula $^{2}_{\infty}$ [Ln^{III}(tfBDC)(NO_3)($DMF)_2$]·DMF with Ln = Ce, Pr, Nd, Sm, Dy, Er, Yb.[11] In this work we have now been able to complete the series with most of the missing members of the lanthanide row, i.e. Ln = Eu (1), Gd (2), Tb (3), Ho (4) and Tm (5). So only compounds with the largest (Ln = La) and the smallest lanthanide (Ln = Lu) as well as with radioactive Pm are still unknown. All compounds crystallize in the same structure type in space group *C*2/*c* (No. 15) with $Z = 8$. The unit cell volumes decrease with increasing atomic number as expected for the lanthanide contraction (Figure 1).

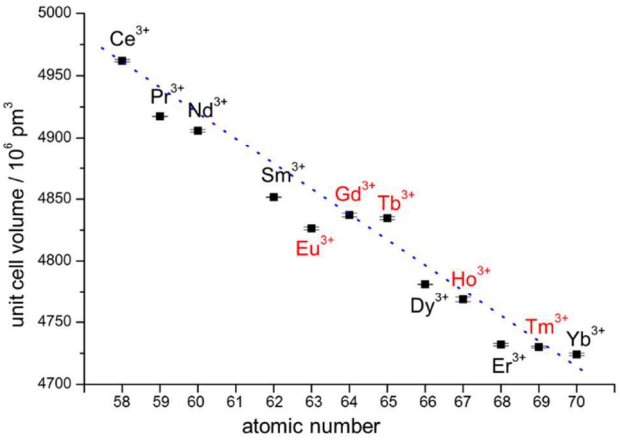

Figure 1: Unit cell volumes of coordination polymers $^{2}_{\infty}$ [Ln^{III}(tfBDC)(NO_3)($DMF)_2$]·DMF; volumes with black atomic symbols are taken from[11], with red symbols: this work. The blue dotted line is a guide for the eye.

As the crystal structure of $^{2}_{\infty}$ [Ln^{III}(tfBDC)(NO_3)($DMF)_2$]·DMF compounds has already been discussed earlier,[11] only a brief description shall be given here taking $^{2}_{\infty}$ [Eu^{III}(tfBDC)(NO_3)($DMF)_2$]·DMF (**1**) as an example for all other isostructural compounds **1-5**. The asymmetric unit of **1** contains one Eu^{3+} cation, one NO_3^- anion and three DMF molecules all on general positions. However, two crystallographically independent $tfBDC^{2-}$ anions are found. Both are located on symmetry elements (inversion center and two-fold axis, resp.), so that the full anion is generated by these symmetry elements. In Figure 2 the coordination sphere around one Eu^{3+} cation is shown. Eu^{3+} is coordinated by nine oxygen atoms (CN = 9) stemming from three monodentately coordinating carboxylate groups of the $tfBDC^{2-}$ ligand (Eu-O: 238.9(4) – 239.7(4) pm), one chelating bidentately coordinating carboxylate group of the $tfBDC^{2-}$ ligand (Eu-O: 249.9(4) and 262.3(3) pm), one chelating bidentately coordinating NO_3^- anion (Eu-O: 250.0(5) and 252.6(4) pm) and two coordinating DMF molecules (Eu-O: 238.7(4) und 239.6(5) pm). The next-nearest distance is Eu-C7 with 291.2(4) pm. The EuO_9 polyhedra are linked by a common edge and bridged by the carboxylate groups of two $tfBDC^{2-}$ ligands to form dimeric units (Figure S22, Supporting Information). The Eu-Eu distance within these dimers is 406.67(8) pm. For comparison, in elemental Europium the shortest Eu-Eu distance is 396 pm. In the series of the coordination polymers $^{2}_{\infty}$ [Ln^{III}(tfBDC)(NO_3)($DMF)_2$]·DMF the Ln^{III}-Ln^{III} distances decrease with increasing atomic number (Table 3). The same trend is found for the Ln^{III}-O distances (Table 3). These dimeric ($EuO_{7/1}O_{2/2})_2$ units are connected via the $tfBDC^{2-}$ ligands to form sheets with distorted square grids in the (100) plane (Figure S23, Supporting Information). One $tfBDC^{2-}$ ligand connects along [010] and the other along [001]. These layers are stacked along [100] in an AB fashion with a translation vector ~½ ½ 0, so that the dimers of the next layer are not positioned above the center of the square grids of the layer below, but above their edges. The layers are held together by weak van der Waals forces. Non-coordinated DMF molecules fill the space in-between the layers, but also the space within the square grids so that no pores are found in this coordination polymer.

It has been shown earlier[10] that the benzene rings and carboxylate groups are not coplanar in tetrafluoroterephthalates due to an electrostatic repulsion between the fluorine atoms on the ring and the oxygen atoms of the carboxylate groups as well as a decrease in aromatic character of the carboxylate group due to the electron-withdrawing nature of the fluorine atoms.[23,24] Therefore torsion angles between the benzene rings and the carboxylate groups of 79.0(2)° (2x), 48.1(4)° and 52.1(4)° are found for the two crystallographically independent $tfBDC^{2-}$ ligands in **1**. For symmetry reasons the carboxylate groups themselves are coplanar in $tfBDC^{2-}$ ligand 1, whereas a slight tilting of ~4° is found in ligand 2.

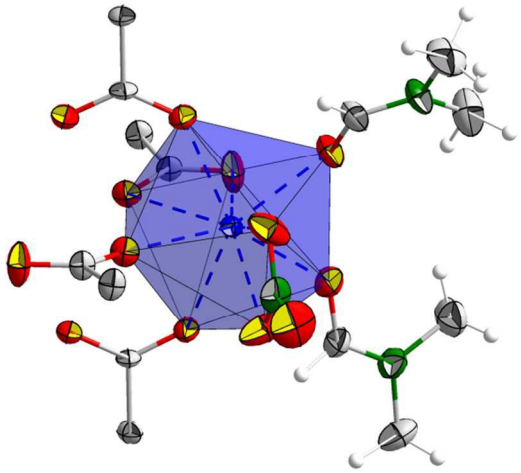

Figure 2: ORTEP plot (50 % probability) of the coordination sphere around Eu^{3+} in $^{2}_{\infty}[Eu^{III}(tfBDC)(NO_3)(DMF)_2]\cdot DMF$ (**1**); Eu (blue), O (red), C (light gray), N (green), H (small white spheres); the $tfBDC^{2-}$ ligand is only partly depicted.

The thermal stability of compounds 1-5 was investigated by DTA/TGA (Figure 3 and Figures S6 – S9, Supporting Information). All compounds are stable up to approx. 100 °C with the exception of the Tm compound (5), which starts to decompose slightly below 100 °C (Figure S9). As an example the DTA/TGA of 3 shall be discussed in more detail (Figure 3). A broad endothermic signal is observed between 150 °C and 200 °C. The mass loss of approx. 20 % is in good agreement with the release of two DMF molecules (calculated mass loss: 21.6 %). The third DMF molecule is obviously released during the strong exothermic event between 350 °C and 400 °C. The observed mass loss of approx. 35 % points to a decomposition of the framework. The remaining mass at 450 °C (45 % ≡ ~ 304 g/mol) is too high for simple residues like Tb_2O_3 (M/2 = 182.9 g/mol) or TbOF (M = 193.9 g/mol). Roughly similar results were obtained for compounds 1, 2, 4 and 5 (Figures S6 – S9, Supporting Information). Nice plateaus after DMF release are observed for 4 and 5. Thus, 3-5 are good candidates to follow the DMF release via temperature dependent XRPD, as for lower DMF contents a higher connectivity of the framework is expected. But also with respect to the luminescence properties of 3 (see below) a compound with a lower DMF content seems to be very interesting. Thus, these investigations are part of our current research interests in this field. For 1 and 2 less pronounced DTA/TGA curves are found, so that such investigations are less promising for these compounds.

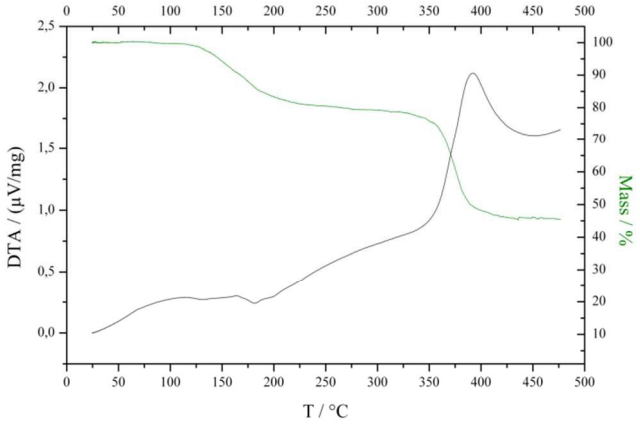

Figure 3: DTA (black) and TGA (green) analysis of $^{2}_{\infty}[Tb^{III}(tfBDC)(NO_3)(DMF)_2]\cdot DMF$ (**3**).

Attempts to crystallize new coordination polymers under similar conditions as for 1-5 just by replacing DMF by formamide (FA) failed. But using a mechanochemical approach starting from the acetates and H_2tfBDC (see Experimental Section) led to the new compounds $^{2}_{\infty}[Ln^{III}(tfBDC)(CH_3COO)(FA)_3]\cdot 3FA$ with $Ln^{III} = Sm^{3+}$ (6) and Eu^{3+} (7). Both are isostructural ($P\bar{1}$, Z = 2) so that only compound 7 shall be discussed in detail. The asymmetric unit of 7 consists of one Eu^{3+} cation, one CH_3COO^- anion and six formamide molecules all on general positions. Two crystallographically independent $tfBDC^{2-}$ anions are found. However, both are located on inversion centers, so that the full linkers are generated by this symmetry element. In Figure 4 the coordination sphere around one Eu^{3+} cation is shown. Eu^{3+} is coordinated by nine oxygen atoms (CN = 9) stemming from three monodentately coordinating carboxylate groups of the $tfBDC^{2-}$ ligand (Eu-O: 235.6(2) – 245.9(2) pm), one chelating bidentately coordinating (Eu-O: 252,7(2) pm and 259.4(2) pm) and one monodentately coordinating (Eu-O: 237.2(2) pm) carboxylate groups of acetate anions, and three coordinating formamide (FA) molecules (Eu-O: 242.1(2) pm – 250.4(2) pm). The next-nearest distance is Eu-C12 with 294.8(2) pm. The EuO_9 polyhedra are linked by a common edge and bridged by the carboxylate groups of two acetate anions to form dimeric units (Figure 5). The Eu-Eu distance within these dimers is 405.85(3) pm (Eu-Eu in 1: 406.67(8) pm). The Sm-Sm distances in 6 are, as expected, slightly larger: 408.05(7) pm. The same is found for the Sm-O distances (Table 3).

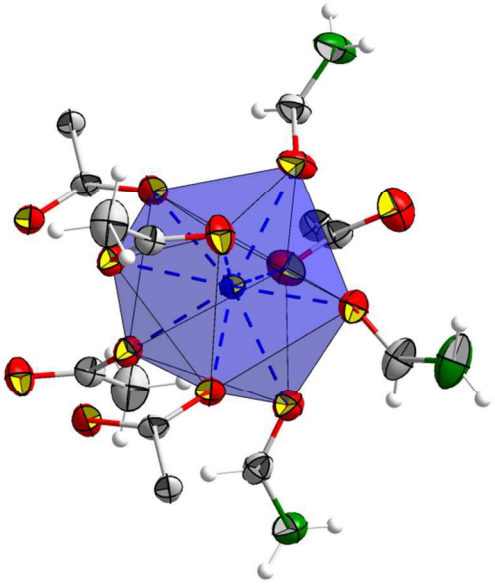

Figure 4: ORTEP plot (50 % probability) of the coordination sphere around Eu^{3+} in $^{2}_{\infty}[Eu^{III}(tfBDC)(CH_3COO)(FA)_3]\cdot 3FA$ (**7**); Eu (blue), O (red), C (light gray), N (green), H (small white spheres); the $tfBDC^{2-}$ ligand is only partly depicted.

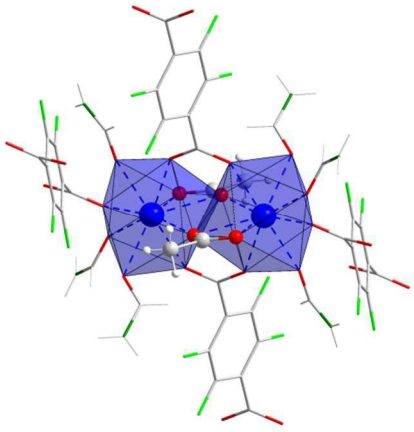

Figure 5: Dimeric units in $^{2}_{\infty}[Eu^{III}(tfBDC)(CH_3COO)(FA)_3]\cdot 3FA$ (**7**); Eu^{3+} and CH_3COO^- are shown as balls and sticks, formamide

(FA) and $tfBDC^{2-}$ as wires/sticks; Eu (blue), O (red), C (light gray), N (green), F (light green), H (white).

The dimeric $(EuO_{7/1}O_{2/2})_2$ units are connected via the $tfBDC^{2-}$ ligands to form sheets, which are shown in Figure 6. These layers are stacked along [010] in an AA fashion. The layers are held together by weak van der Waals forces. Non-coordinated formamide (FA) molecules (three per formula unit) fill the space in-between the layers so that no pores are found in this coordination polymer. Torsion angles between the benzene rings and the carboxylate groups of 69.3(1)° (2x) and 62.9(1)° (2x) are found for the two crystallographically independent $tfBDC^{2-}$ ligands. For symmetry reasons the carboxylate groups themselves are coplanar in both $tfBDC^{2-}$ ligands.

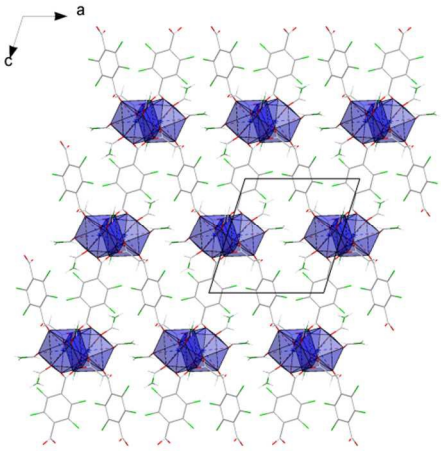

Figure 6: View of a polymeric layer in the crystal structure of $^2_\infty[Eu^{III}(tfBDC)(CH_3COO)(FA)_3]\cdot 3FA$ (**7**) along [010]; all atoms and bonds are shown in a wires/sticks representation; non-coordinating formamide (FA) molecules are omitted for clarity; color coding as in Figure 5.

The DTA/TGA curves of **6** and **7** are given in the Supporting Information (Figures S13 and S14). Release of formamide molecules starts slightly above 100 °C. For **7** a release of one formamide molecule should lead to a mass loss of 6.3 %. So at approx. 200 °C the release of six formamide molecules seems to be finished. But as no clear plateau is reached, the solvent release seems to overlap with the decomposition of the framework. The remaining masses for **6** (approx. 30 % at 500 °C) and **7** (approx. 43 % at 300 °C) are higher than the expected values for ½ $Ln^{III}_2O_3$ (~24.5 %) and $Ln^{III}OF$ (~26 %). Thus, the mechanism of the decomposition is unclear at the moment.

Single crystals of compounds $^2_\infty[Ln^{III}(tfBDC)(NO_3)(DMSO)_2]$ with $Ln^{III} = Ho^{3+}$ (**8**), Er^{3+} (**9**) and Tm^{3+} (**10**) were obtained under similar conditions as compounds **1**-**5** by replacing DMF by DMSO. All compounds are isostructural (*Pbca*, Z = 8) so that only compound **10** shall be discussed in the following. The asymmetric unit of **10** consists of one Tm^{3+} cation, one $tfBDC^{2-}$ anion, one NO_3^- anion and two DMSO molecules all on general positions. In Figure 7 the coordination sphere around one Tm^{3+} cation is shown. Tm^{3+} is coordinated by eight oxygen atoms (CN = 8) stemming from four monodentately coordinating carboxylate groups of the $tfBDC^{2-}$ ligand (Tm-O: 228.0(3) – 234.9(3) pm), one chelating bidentately coordinating nitrate anion (Tm-O: 241.4(3) pm and 242.3(3) pm), and two coordinating DMSO molecules (Tm-O: 227.7(3) pm and 230.1(3) pm). The next-nearest distance is Tm-N3 with 283.7(5) pm. In contrast to compounds **1**-**7** these TmO_8 polyhedra are not linked directly, but bridged by chelating carboxylate groups of four $tfBDC^{2-}$ ligands (Figure 8). Thus, a paddlewheel-like unit is formed. But as the $tfBDC^{2-}$ anions are not coplanar for reasons mentioned above (torsion angles between the benzene ring and the carboxylate groups: 71.1(2)° and 77.2(2)°; torsion angle between both carboxylate groups: ~9°), the paddles of the paddlewheel are not parallel to its axis, but almost perpendicular to it. The Tm-Tm distance within these dimers is significantly enhanced compared to **1**-**7** (Table 3): Tm-Tm = 439.48(5) pm in **10** compared to Eu-Eu = 405.85(3) pm in **7** and 406.67(8) pm in **1**. The Ln^{III}-Ln^{III} distances as well as the Ln^{III}-O distances in **8** and **9** are, as expected, slightly larger than in **10** (Table 3). It is noteworthy that the spread of the Ln^{III}-O distances in **8**-**10** is significantly smaller than in compounds **1**-**7** (Table 3). This points to a higher symmetric coordination sphere around Ln^{3+} in **8**-**10** and might be attributed to the fact that no non-coordinating solvent molecules are found in these compounds.

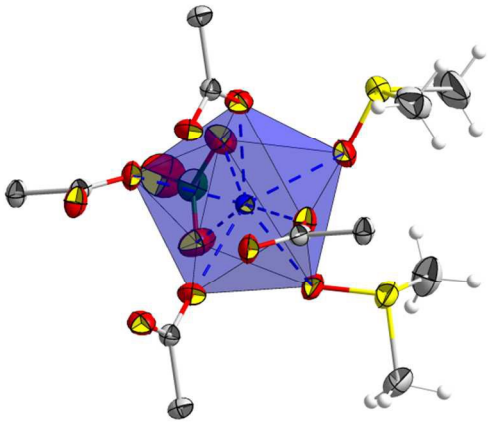

Figure 7: ORTEP plot (50 % probability) of the coordination sphere around Tm^{3+} in $^2_\infty[Tm^{III}(tfBDC)(NO_3)(DMSO)_2]$ (**10**); Tm (blue), O (red), C (light gray), N (green), S (yellow), H (small white spheres); the $tfBDC^{2-}$ ligand is only partly depicted.

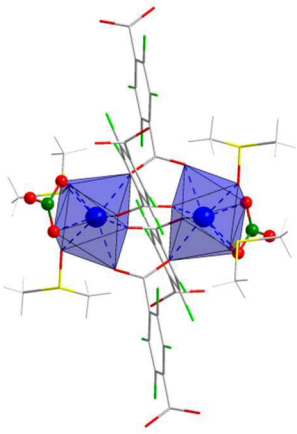

Figure 8: Dimeric units in $^2_\infty[Tm^{III}(tfBDC)(NO_3)(DMSO)_2]$ (**10**); Tm^{3+} and NO_3^- are shown as balls and sticks, DMSO and $tfBDC^{2-}$ as wires/sticks; Tm (blue), O (red), C (light gray), N (green), F (light green), S (yellow), H (white).

The dimeric $(TmO_8)_2$ units in **10** are connected via the $tfBDC^{2-}$ ligands to form sheets in the (001) plane, which are shown in Figure 9. These 4^4 nets are stacked along [001] in an AB fashion with a translation vector ~½ ½ ½, so that the dimers of the next layer are positioned above the center of the square grids of the layer below. The layers are held together by weak van der Waals forces. In Figure S24 (Supporting Information) a space-filling presentation of these layers is given. No non-coordinating solvent molecules are found to fill the empty space shown in Figure S24 (cp. low residual electron density given in Table 2). Thus, compounds **8-10** might be candidates to show permanent porosity and gas sorption properties. Such properties have already been found for similar systems composed of polymeric layers.[25] Such investigations on compounds **8-10** will be performed in the near future.

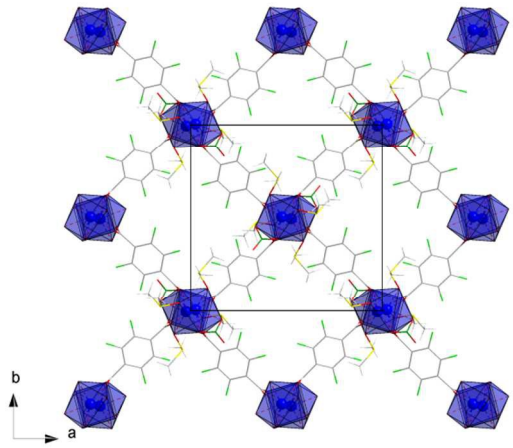

Figure 9: View of a polymeric layer in the crystal structure of $^2_\infty[Tm^{III}(tfBDC)(NO_3)(DMSO)_2]$ (**10**) along [001]; all atoms with the exception of Tm and bonds are shown in a wires/sticks representation; color coding as in Figure 8.

The DTA/TGA curves of compounds **9** and **10** are given in the Supporting Information (Figures S19 and S20). **9** and **10** are more stable than **1-7**. The release of solvents molecules starts above 150 °C. This is due to the fact that the crystal structures of **9** and **10** do not contain non-coordinating solvent molecules like **1-7**. For **10** (**9** shows similar results) an endothermic event is found around 200 °C with a mass loss of approx. 12.8 %. For the loss of one DMSO molecule a mass loss of 12.5 % is calculated. An almost flat plateau after the release of one DMSO molecule makes **10** an interesting candidate to follow the DMSO release via temperature dependent XRPD, as for lower DMSO contents a higher connectivity of the framework can be expected. A second, strong exothermic event is observed at approx. 370 °C. The high mass loss points to a release of the second DMSO molecule accompanied by a decomposition of the compound. The remaining mass at 450 °C (47 % ≡ ~ 293 g/mol) is too high for simple residues like Tm_2O_3 (M/2 = 192.9 g/mol) or TmOF (M = 203.9 g/mol). To analyze this residue **9** was heated to 500 °C in an argon atmosphere. Elemental (CHNS) analysis of the resulting black powder gave approx. 17 weight % carbon, but no nitrogen, sulfur or hydrogen. The XRPD (ESI: Figure S30) of this residue showed several broad reflections, which can be assigned to ErF_3. Only one very broad reflection at $2\theta \approx 4.7°$ seems to belong to rhombohedral graphite, which explains the carbon found in the elemental analysis.

To sum up the crystal structure analyses all known crystal structures of coordination polymers containing Ln^{3+} cations and $tfBDC^{2-}$ linkers shall be compared.[7,11,12,26-28] They are summarized in Table 4. Surprisingly, only in our work[11,this work] it was found that additional anions like NO_3^- or CH_3COO^- are incorporated in the crystal structures of the coordination polymers. Larionov et al. started from freshly prepared $Ln(OH)_3$,[26,27] but in the work of Mikhalyova et al.,[28] MacNeill et al.,[12] and Chen et al.[7] synthetic procedures similar to ours were used. So the choice of the solvents – addition of water,[7] MeOH instead of EtOH,[28] or DEF instead of DMF[12] – and the reaction temperature - 80 °C in Ref. 7, all others at RT – seem to influence the incorporation of NO_3^- anions, as the solubility of the nitrates is changed. Our new mechanochemical synthesis starting from $Ln(CH_3COO)_3\ H_2O$ and H_2tfBDC seems to be an interesting approach to incorporate acetate anions.[this work] The coordination numbers of the Ln^{3+} cations mainly follow the size of the cations: for the larger lanthanides CN = 9 is preferred, whereas for the smaller lanthanides also CN = 8 is found. Only the structure type $^2_\infty[Ln^{III}(tfBDC)(NO_3)(DMF)_2]\cdot DMF$ (type IV, Table 4) seems to be very flexible, as here CN = 9 is found for almost all lanthanides.[11,this work] A common feature of all compounds are binuclear units, which seem to be a preferred structural unit in the crystal chemistry of coordination polymers with Ln^{3+} and $tfBDC^{2-}$ linkers. In all types (Table 4) with the exception of type I these binuclear units are connected by $tfBDC^{2-}$ ligands in two directions to form a layer-like polymer. But despite these similarities, in detail the dimers differ significantly with respect to coordination number, surrounding of Ln^{3+} cations and connection of the monomers to dimers (connection via edges in types III, IV, VI and via faces in types II, VII; the different connectivity of type V is shown in Figure 8). Most strikingly, the stacking of the layers is different, as shown for compounds **1-10** in this manuscript. But still, at the moment the crystal chemistry of coordination polymers with Ln^{3+} and $tfBDC^{2-}$ linkers is less multifaceted as that of coordination polymers of Ln^{3+} and non-fluorinated BDC^{2-} linkers, as described by Mikhalyova et al..[28] The only 3D polymer up to now is $^3_\infty[Er(tfBDC)_{3/2}(DMF)_{1/2}(H_2O)_{1/2}]$ ½ DMF (type I).[7] Here, $(Er1)_2$ (Er1-Er1: 378.35(5) pm) and $(Er2)_2$ dimers (Er2-Er2: 379.91(5) pm) connected via common edges are further connected to rod-like chains by two bridging carboxylate groups of the $tfBDC^{2-}$ ligands (Er1-Er2: 500.33(7) pm). These rods are interconnected by $tfBDC^{2-}$ ligands in two directions to form a 3D framework structure.

It was already shown that coordination polymers with perfluorinated linkers give rise to strong emission, as quenching due C-H-related vibronic states is reduced.[7,11] Previous work, however, was restricted to Pr^{3+}, Sm^{3+}, Dy^{3+}, and Er^{3+} containing compounds. Bright red and green photoluminescence of Eu^{3+} and Tb^{3+} containing coordination polymers has also been investigated.[12,26,27] But to the best of our knowledge, a quantitative analysis of the quantum yield has never been performed up to now. Irradiating the compounds **1** and **3** with UV light as well resulted in a bright red (**1**) and green (**3**) luminescence, as shown in the insets of Figures 10 and 11. Excitation spectra of **1** (ESI: Figure S25) show that the maximum emission band with Λ_{max} = 618 nm was excited. The spectrum shows the typical $^5D_0 \rightarrow {}^7F_2$ transition, also known as hypersensitive electric dipole transition that is characteristic for Eu^{3+} ions located on centers of symmetry, as found in the crystal structure of **1**. Further excitation bands were observed for $^5D_1$, $^5D_0$, $^5L_6$, $^5G_2$, $^5L_7$, $^5G_{3,4,5,6}$ and $^5D_4$ transitions. A broad band around 298 nm indicates the absorption of the $tfBDC^{2-}$ linker.

The emission spectrum of **1** (Figure 10; Λ_{ex} = 393 nm) reveals several f-f-transitions $^5D_0 \rightarrow {}^7F_J$ with J = 0, 1, 2, 3, 4. The most intensive band arises from the hypersensitive transition $^5D_0 \rightarrow {}^7F_2$ (619 nm), which is, as mentioned, very sensitive to its chemical environment and responsible for the bright red color of the

luminescence. Further weaker emission bands were observed at Λ_{em} = 686/697 nm ($^5D_0 \rightarrow {}^7F_4$), at 650 nm ($^5D_0 \rightarrow {}^7F_3$) and at 590/593 nm ($^5D_0 \rightarrow {}^7F_1$). $^5D_0 \rightarrow {}^7F_1$ and $^5D_0 \rightarrow {}^7F_3$ transitions are magnetic dipole transitions that are independent of their chemical environment, so that it is possible to use their intensities as a standard to compare the intensities of other transitions.

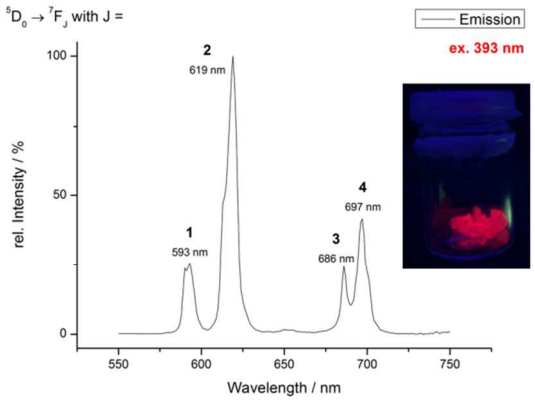

Figure 10: Emission spectrum of **1** (Λ_{ex} = 393 nm); inset: intense red emission of single crystals of **1**.

The relative quantum yields were determined with an integrating sphere („Ulbricht sphere"). During a day a decrease of the quantum yield from 45 % to 9 % was observed. After one hour at 60 °C, a maximum quantum yield of 53 % was obtained. The DTA/TG curve of **1** reveals that the sample is stable up to 100 °C and higher. So we assume that **1** takes up water from the atmosphere, which quenches the luminescence via O-H vibrations. Attempts to excite **1** via the $tfBDC^{2-}$ linker have not been successful up to now. But this is part of our ongoing work in this field with a special focus on energy transfer via the linker to the next Ln^{3+} center.

Excitation and emission spectra of **3** (ESI: Figure S26, Figure 11) show typical Tb^{3+} transitions. If excited at 378 nm, the following transitions occur: $^5D_4 \leftarrow {}^7F_6$, $^5D_3 \leftarrow {}^7F_6$, $^5G_6 \leftarrow {}^7F_6$, $^5L_{10} \leftarrow {}^7F_6$, $^5G_5 \leftarrow {}^7F_6$, $^5L_9 \leftarrow {}^7F_6$, $^5G_4 \leftarrow {}^7F_6$, $^5D_1 \leftarrow {}^7F_6$ and $^5D_2 \leftarrow {}^7F_6$. The absorption band of the $tfBDC^{2-}$ linker overlaps with the strong and broad $^5D_1 \leftarrow {}^7F_6$ transition. Only a weak shoulder at 298 nm is observed. The emission spectrum of **3** (Λ_{ex} = 378 nm) is dominated by a strong band at 544 nm that is responsible for the bright green emission. The following transitions are observed: $^5D_4 \rightarrow {}^7F_J$ with J = 1, 2, 3, 4, 5, 6. The first two are very weak, whereas the transition with J = 5 gives rise to the strong band at 544 nm.

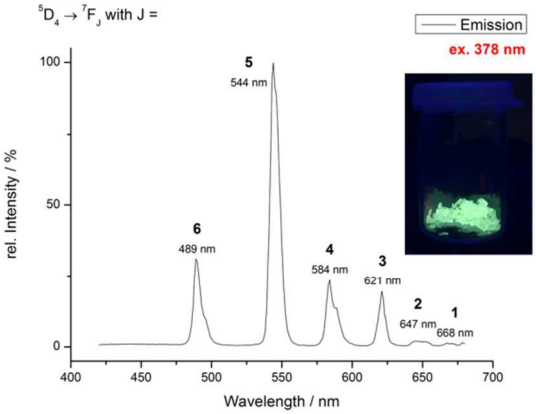

Figure 11: Emission spectrum of **3** (Λ_{ex} = 378 nm); inset: intense green emission of single crystals of **3**.

As maximum quantum yield for **3**, we obtained 67 %. Similar to **1** the quantum yield decreases if exposed to air for longer times. The quantum yield of a sample having the minimum quantum yield of 35 % was heated at 60 °C for one hour, which increased the quantum yield to 49 %. Like for **1**, we assume that moisture from the atmosphere decreases the quantum yield by O-H quenching significantly. These results were obtained for samples containing larger crystals. But measurements on powdered samples gave similar results with a lower quantum yield, in general. Again, attempts to excite **3** via the $tfBDC^{2-}$ linker have not been successful up to now.

To investigate the influence of solvent molecules on the luminescence properties, excitation (Figure S27, Supporting Information) and emission spectra (Figure 12) of **7** were recorded. Like compound **1**, **7** contains Eu^{3+} cations and $tfBDC^{2-}$ linkers, but NO_3^- is replaced by CH_3COO^-, and DMF by formamide. Based on the simple picture of C-H-related quenching, one expects a weaker luminescence of **7**, as CH_3COO^- is coordinating directly to Eu^{3+}. This expectation is fulfilled, as a quantum yield as low as 10% was observed for **7**. The excitation spectrum of **7**, measured at $\Lambda_{em,max}$ = 618 nm, shows the following transitions: $^5D_1$, $^5D_0$, $^5L_6$, $^5G_2$, $^5L_7$, $^5L_6$, $^5G_{3,4,5,6}$, $^5D_4$ as well as a broader band at 317 nm that could not be assigned to any reasonable transition. The absorption band of the $tfBDC^{2-}$ linker seems to start below 300 nm and is thus significantly shifted as compared to **1**. The emission spectrum of **7** (Figure 12), excited at 393 nm, shows $^5D_0 \rightarrow {}^7F_J$ transitions with J = 1-4. The most intensive band at Λ_{max} = 592 nm (J = 1) is surprisingly stronger than the band at 618 nm (J = 2). The latter is a hypersensitive transition, typical for Eu^{3+}.

Figures S28 and S29 (Supporting Information) show comparisons of the excitation and emission spectra of **1** and **7**, setting the strongest band of each spectrum to 100 %. Different intensities indicate different coordination spheres and symmetries in both compounds. In the excitation spectra a broad band for the $tfBDC^{2-}$ linker at 298 nm for **1** seems to be shifted to higher energies for **7**. Furthermore, the intensity of the $^5D_0 \rightarrow {}^7F_2$ transition in **1** (emission spectrum) is significantly higher than in **7**, which is also reflected in the higher quantum yield of **1** compared to **7**.

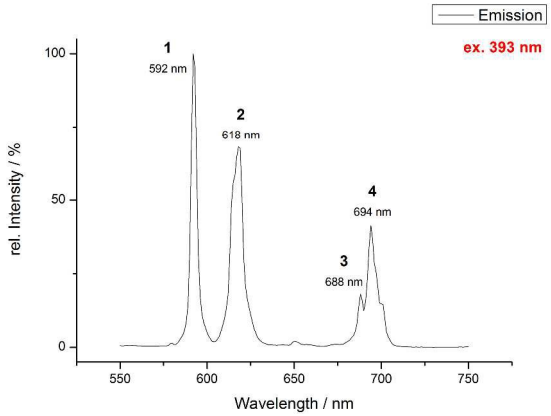

Figure 12: Emission spectrum of **7**.

Experimental

General Remarks

Tetrafluoroterephthalic acid (H_2tfBDC) was prepared according to the procedure described in the literature.[9]
$Er(NO_3)_3 \cdot 5H_2O$, $Eu(CH_3COO)_3 \cdot H_2O$, $Eu(NO_3)_3 \cdot 6H_2O$, $Gd(NO_3)_3 \cdot 6H_2O$, $Ho(NO_3)_3 \cdot 5H_2O$, $Sm(CH_3COO)_3 \cdot H_2O$, $Tb(NO_3)_3 \cdot 6H_2O$, $Tm(NO_3)_3 \cdot 6H_2O$ (all from ABCR), *N,N'*-dimethylformamide (KMF LaborchemieHandels GmbH), formamide (Alfa Aesar), dimethyl sulfoxide (VWR BDH Prolabo), ethanol (Biesterfeld) and triethylamine (Acros Organics) were used as purchased, without any further purification. In all syntheses, yields were not optimized and, therefore, are not given.

Syntheses

Compounds with composition $^2_\infty$ $[Ln^{III}(tfBDC)(NO_3)(DMF)_2] \cdot DMF$ with $Ln^{III} = Eu^{3+}$ (**1**), Gd^{3+} (**2**), Tb^{3+} (**3**), Ho^{3+} (**4**) and Tm^{3+} (**5**) were synthesized as follows:
1.5 mmol, (1.4 equiv.) $Ln^{III}(NO_3)_3 \cdot xH_2O$ and 1.1 mmol (1.0 equiv.) H_2tfBDC were dissolved in 10 mL of a solvent mixture of ethanol and *N,N'*-dimethylformamide (3:1,v:v). The snap-cap tube was closed with a cap and the latter was perforated once. It was placed in an exsiccator, whose bottom was filled with 100 mL of the solvent mixture mentioned above. In addition, a beaker with 20 mL of triethylamine dissolved in 20 mL of the same solvent mixture was placed in the exsiccator. After one month, colorless crystals of **1**, **2**, **3** and **5** and pink crystals of **4** several millimeters in size were obtained.
Elemental analysis for **1**: Found: C, 29.7; H, 3.5; N, 8.6. Calc. for $EuC_{17}H_{21}O_{10}F_4N_4$: C, 30.5; H, 3.2; N, 8.4. Purity was additionally checked by XRPD (Figure S1 in the Supporting Information). Both investigations indicate that a single-phase sample was obtained.
Elemental analysis for **2**: Found: C, 29.9; H, 3.6; N, 8.6. Calc. for $GdC_{17}H_{21}O_{10}F_4N_4$: C, 30.3; H, 3.1; N, 8.3. Purity was additionally checked by XRPD (Figure S2 in the Supporting Information). Weak additional reflections indicate a small amount of an unknown impurity. Therefore, only the results of the X-ray single-crystal structure analysis of **2** are discussed in the following.
Elemental analysis for **3**: Found: C, 30.4; H, 3.6; N, 8.1. Calc. for $TbC_{17}H_{21}O_{10}F_4N_4$: C, 30.2; H, 3.1; N, 8.2. Purity was additionally checked by XRPD (Figure S3 in the Supporting Information). Both investigations indicate that a single-phase sample was obtained.
Elemental analysis for **4**: Found: C, 28.7; H, 3.3; N, 7.4. Calc. for $HoC_{17}H_{21}O_{10}F_4N_4$: C, 29.9; H, 3.1; N, 8.2. Purity was additionally checked by XRPD (Figure S4 in the Supporting Information). The latter does not show any impurity reflections, but due to the modest elemental analysis only the results of the X-ray single-crystal structure analysis of **4** are discussed in the following.
Elemental analysis for **5**: Found: C, 28.2; H, 3.1; N, 6.8. Calc. for $TmC_{17}H_{21}O_{10}F_4N_4$: C, 29.8; H, 3.1; N, 8.2. Purity was additionally checked by XRPD (Figure S5 in the Supporting Information). Both investigations indicate that no single-phase sample was obtained. Therefore, only the results of the X-ray single-crystal structure analysis of **5** are discussed in the following.
IR data (KBr pellets) of **1**-**5** are presented in Figure S10 and Table S1 in the Supporting Information.
Compounds with composition $^2_\infty$ $[Ln^{III}(tfBDC)(CH_3COO)(FA)_3] \cdot 3FA$ with $Ln^{III} = Sm^{3+}$ (**6**) and Eu^{3+} (**7**) were synthesized applying a mechanochemical approach: 3 mmol, (2.0 equiv.) $Ln^{III}(CH_3COO)_3 \cdot H_2O$ were ground with 1.5 mmol (1.0 equiv.) H_2tfBDC, until no smell of acetic acid was noticed any longer. The residue was dissolved in 60 ml formamide (FA). After approx. one week single crystals of **6** and **7** were obtained after slow evaporation of the solvent.
Elemental analysis for **6**: Found: C, 26.4; H, 2.7; N, 11.9. Calc. for $SmC_{16}H_{21}F_4N_6O_{12}$: C, 26.9; H, 3.0; N, 11.7. Purity was additionally checked by XRPD (Figure S11 in the Supporting Information). Both investigations indicate that a single-phase sample was obtained.
Elemental analysis for **7**: Found: C, 26.4; H, 3.0; N, 11.1. Calc. for $EuC_{16}H_{21}F_4N_6O_{12}$: C, 26.8; H, 3.0; N, 11.7. Purity was additionally checked by XRPD (Figure S12 in the Supporting Information). Both investigations indicate that a single-phase sample was obtained.
IR data (KBr pellets) of **6** and **7** are presented in Figure S15 and Table S2 in the Supporting Information.
Compounds with composition $^2_\infty$ $[Ln^{III}(tfBDC)(NO_3)(DMSO)_2]$ with $Ln^{III} = Ho^{3+}$ (**8**), Er^{3+} (**9**) and Tm^{3+} (**10**) were synthesized by a similar synthesis described for compounds **1-5**. 1.5 mmol, (1.4 equiv.) $Ln^{III}(NO_3)_3$ x H_2O and 1.1 mmol (1.0 equiv.) H_2tfBDC were dissolved in 10 mL of a solvent mixture of ethanol and dimethyl sulfoxide (3:1, v:v). The snap-cap tube was closed with a cap and the latter was perforated once. It was placed in an exsiccator, whose bottom was filled with 100 mL of the solvent mixture mentioned above. In addition, a beaker with 20 mL of triethylamine dissolved in 20 mL of the same solvent mixture was placed in the exsiccator. After 1-2 months pink crystals of **8** and **9** and colourless crystals of **10** were obtained.
Elemental analysis for **8**: Found: C, 23.1; H, 2.5; N, 2.5; S, 10.1. Calc. for $HoC_{12}F_4S_2O_9N$: C, 23.3; H, 2.0; N, 2.6; S, 10.4. Purity was additionally checked by XRPD (Figure S16 in the Supporting Information). Both investigations indicate that a single-phase sample was obtained.
Elemental analysis for **9**: Found: C, 22.2; H, 2.5; N, 2.2; S, 7.9. Calc. for $ErC_{12}F_4S_2O_9N$: C, 23.2; H, 2.0; N, 2.3; S, 10.3. Purity was additionally checked by XRPD (Figure S17 in the Supporting Information). Both investigations indicate that no single-phase sample was obtained.
Elemental analysis for **10**: Found: C, 22.3; H, 2.3; N, 2.3; S, 7.1. Calc. for $TmC_{12}F_4S_2O_9N$: C, 23.1; H, 1.9; N, 2.3; S, 10.3. Purity was additionally checked by XRPD (Figure S18 in the Supporting Information). The elemental analysis indicates that no single-phase sample was obtained.
IR data (KBr pellets) of **8**-**10** are presented in Figure S21 and Table S3 in the Supporting Information.

X-Ray Single Crystal Structure Analysis

Single crystals of **1**−**10** were isolated and mounted in sealed glass capillaries on a Stoe IPDS I or IPDS II diffractometer ($T \approx 293$ K, Mo Kα radiation). For data collection and reduction the Stoe program package[13] was applied. The structural models were solved using SIR-92[14] and completed using difference Fourier maps calculated with SHELXL-97,[15] which was also used for final refinements. These programs were run under the WinGX system.[16] All non-hydrogen atoms were refined anisotropically. Hydrogen atoms of solvent molecules and acetate groups were placed on calculated positions and refined "riding" with fixed distances (93 pm (C(O)H group), 96 pm (CH_3 group), 86 pm (NH_2 group)). Details of all single-crystal structure analyses are given in Tables 1 and 2.[17]

X-Ray Powder Diffraction

XRPD data were collected at room temperature on a Huber G670 diffractometer (germanium monochromator, $CuK\alpha_1$ radiation, imaging plate detector). To minimize the strong absorption of all compounds, measurements were carried out as flat samples with the substances placed between two foils (reflections due to the foil: $2\theta \approx 21.5°$ and $2\theta \approx 23.7°$). Typical

recording times range from 60 min (compounds **6** and **7**) to 720 min (compounds **1**–**5** and **8**–**10**). Employing the WinXPow software suite,[18] the recorded patterns were compared with theoretical patterns calculated from single-crystal structure data.

Elemental Analysis

Elemental analyses were carried out with a HEKAtech CHNS Euro EA 3000.

Thermoanalytical Investigations

Differential thermal analyses (DTA) and thermogravimetric analyses (TGA) were performed in Al_2O_3 containers (typical sample masses: approx. 20 mg). The temperature intervals were 25-300 °C and 25-500 °C, resp. with heating rates of 10-20 °C/min. The instrument (Netzsch STA 409C) is housed in a glovebox (M. Braun, Garching/Germany, nitrogen atmosphere) and the sample chamber is continuously flushed with argon with a rate of 70 ml/min.

Infrared Spectroscopy

IR measurements were carried out on KBr pellets using a Bruker IFS 66v/S with a Nernst globar.

Absorption

Visible and NIR absorption spectra were measured at room temperature on a Cary 5000 spectrometer (Varian, Palo Alto, USA). For the measurements, pellets of solid samples were prepared and fixed in the sample holder.

Luminescence Spectroscopy

Excitation and emission spectra were recorded using a HORIBA Jobin Yvon Fluorolog 3 photoluminescence spectrometer equipped with a continuous 450 W xenon lamp, double monochromators for excitation and emission beam, an integrating sphere (Ulbricht sphere), and a photomultiplier tube (PMT) as the detector. Excitation and emission spectra were corrected using standard corrections, including the spectral intensity distribution of the lamp, the reflection behavior of the Ulbricht sphere, and the sensitivity of the detector. Determination of the absolute quantum yield was performed as suggested by Friend and co-workers.[20,21,22] All samples were investigated as solids in spectroscopically pure quartz cuvettes in the front-face mode. For the measurements, crystals were freshly taken from the supernatant solvent mixture, dried with tissue, ground and filled in the cuvettes.

Conclusion

To conclude, we have been able to synthesize and characterize ten new coordination polymers based on lanthanide cations and tetrafluoroterephthalate ($tfBDC^{2-}$) linkers. Three different structure types were obtained depending on the solvent (DMF, DMSO, formamide) and the anion (NO_3^-, CH_3COO^-). In all compounds binuclear units connected to polymeric layers are found, which however show several differences: e.g. different coordination numbers and different stacking of the layers. Bright luminescence is found in $^2_\infty[Ln^{III}(tfBDC)(NO_3)(DMF)_2]\cdot DMF$ with $Ln^{3+} = Eu^{3+}$(**1**) and Tb^{3+}(**3**). Quantum yields up to 53 % (**1**) and 67 % (**3**) are remarkable. Obviously, the typical C-H quenching in such compounds is significantly reduced by using a perfluorinated linker. In $^2_\infty[Eu^{III}(tfBDC)(CH_3COO)(FA)_3]\cdot 3FA$ (**7**) (FA = formamide) the quantum yield is reduced to only 10 %. This is ascribed to C-H quenching of the coordinating CH_3COO^- anion. In this respect it seems to be worthwhile to determine the quantum yields of other Eu^{3+} [12,26] and Tb^{3+} [12,25] containing coordination polymers with $tfBDC^{2-}$ linkers to investigate the influence of coordinating solvent molecules and additional anions on the luminescence properties in more detail.

In future experiments we are planning to remove DMF in **1** and **3** to obtain compounds with even higher quantum yields. According to DTA/TGA measurements at least two DMF molecules should be removable without decomposing the coordination network. The release of solvent molecules might further lead to compounds with a 3D connected framework. As binuclear units are found in all compounds we have already successfully incorporated two different lanthanide cations in these polymers. Detailed spectroscopic measurements are planned to prove a possible energy transfer between the two lanthanide centers.

Acknowledgements

We thank Dr. Ingo Pantenburg and Mr. Peter Kliesen for collecting X-ray single crystal data, as well as Mrs. Malgorzata Smolarek for DTA/TGA and IR measurements and Mrs. Silke Kremer for elemental analysis. The help of Prof. Dr. Anja-Verena Mudring and Dr. Chantal Lorbeer in recording first preliminary luminescence spectra and helpful discussions for the interpretation of these data is greatly acknowledged.

Notes and references

[a] Department of Chemistry, University of Cologne, Greinstraße 6, D-50939 Cologne, Germany
* E-mail: uwe.ruschewitz@uni-koeln.de
[b] Institute of Inorganic Chemistry, Karlsruhe Institute of Technology (KIT), Engesserstraße 15, D-76131 Karlsruhe, Germany

† Electronic Supplementary Information (ESI) available: Experimental and simulated powder X-ray diffraction patterns, DTA/TGA diagrams, IR spectra/data, excitation spectra, comparison of excitation and emission spectra, additional figures of crystal structures, and X-ray crystallographic files in CIF format of compounds **1**−**10**. See DOI: 10.1039/b000000x/

1 A. K. Cheetham and C. N. R. Rao, *Science*, 2007, **318**, 58.
2 C. Yang, X. Wang, M. A. Omary, *Am. Chem. Soc.*, 2007, **129**, 15454.
3 C. Yang, X. Wang, M. A. Omary, *Angew. Chem. Int. Ed.*, 2009, **48**, 2500.
4 L. Zhang, Q. Wang, Y.-C. Liu, *J. Phys. Chem. B*, 2007**,** **111**, 4291.
5 Z. Hulvey, D. A. Sava, J. Eckert, A. K. Cheetham, *Inorg. Chem.*, 2011, **50**, 403.
6 P. Pachfule, Y. Chen, J. Jiang, R. Banerjee, *Chem. Eur. J.*, 2012, **18**, 688.
7 B. Chen, Y. Yang, F. Zapata, G. Qian, Y. Luo, J. Zhang, E. B. Lobkovsky, *Inorg. Chem.*, 2006, **45**, 8882.
8 R. J. Harper, E. J. Soloski, C. Tamborski, *J. Org. Chem.*, 1964, **29**, 2385.

9 A. Orthaber, C. Seidel, F. Belaj, R. Pietschnig, U. Ruschewitz, *Inorg. Chem.*, 2010, **49**, 9350.
10 C. Seidel, R. Ahlers, U. Ruschewitz, *Cryst. Growth Des.*, 2011, **11**, 5053.
11 C. Seidel, C. Lorbeer, J. Cybińska, A.-V. Mudring, U. Ruschewitz, *Inorg. Chem.*, 2012, **51**, 4679.
12 C. M. MacNeill, C. S. Day, A. Marts, A. Lachgar, R. E. Noftle, *Inorg. Chim. Acta*, 2011, **365**, 196.
13 Stoe, IPDS manual; Stoe & Cie GmbH: Germany; X-Red 1.22Stoe Data Reduction Program; Stoe & Cie GmbH: Germany, 2001.
14 A. Altomare, G. Cascarano, C. Giacovazzo, A. Gualardi, *J. Appl. Crystallogr.*, 1993, **26**, 343.
15 G. M. Sheldrick, *SHELXL-97: A Program for Crystal Structure Refinement*, University of Göttingen: Germany, 1997, release 97-2; G. M. Sheldrick, *Acta Crystallogr.*, 2008, **A64**, 112.
16 WinGX-Version 1.64.04, An Integrated System of Windows Programs for the Solution, Refinement and Analysis of Single Crystal X-Ray Diffraction Data, Department of Chemistry, University of Glasgow: UK, 1997-2002; L. J. Farrugia, *J. Appl. Crystallogr.*, 1999, **32**, 837.
17 Crystallographic data (excluding structure factors) for the structures reported in this paper have been deposited with the Cambridge Crystallographic Data Centre as supplementary publication no. CCDC- 957999 ($^{2}_{\infty}$[Eu(tfBDC)$(NO_3)(DMF)_2$]· DMF, **1**), CCDC-958000 ($^{2}_{\infty}$[Gd(tfBDC)$(NO_3)(DMF)_2$]· DMF, **2**), CCDC-958001 ($^{2}_{\infty}$[Tb(tfBDC)$(NO_3)(DMF)_2$]· DMF, **3**), CCDC-958002 ($^{2}_{\infty}$[Ho(tfBDC)$(NO_3)(DMF)_2$]· DMF, **4**), CCDC-958003 ($^{2}_{\infty}$[Tm(tfBDC)$(NO_3)(DMF)_2$]· DMF, **5**), CCDC-1025456 ($^{2}_{\infty}$[Sm(tfBDC)$(CH_3COO)(FA)_3$]·3FA, **6**), CCDC-1025457 ($^{2}_{\infty}$[Eu(tfBDC)$(CH_3COO)(FA)_3$]·3FA, **7**), CCDC-1025458 ($^{2}_{\infty}$[Ho(tfBDC)$(NO_3)(DMSO)_2$], **8**), CCDC-1025459 ($^{2}_{\infty}$[Er(tfBDC)$(NO_3)(DMSO)_2$], **9**), CCDC-1025460 ($^{2}_{\infty}$[Tm(tfBDC)$(NO_3)(DMSO)_2$], **10**). Copies of the data can be obtained free of charge on application to CCDC, 12 Union Road, Cambridge CB2 1EZ, UK [fax.: (internat.) + 44 1223/336-033; e-mail: deposit@ccdc.cam.ac.uk].
18 *Win XPow*, version 3.03 (06-Dec-2010); Stoe & Cie GmbH: Darmstadt, Germany.
19 (a) R. D. Shannon, C. T. Prewitt, *Acta Crystallogr., Sect. B: Struct. Crystallogr. Cryst. Chem.*, 1969, **B25**, 925; (b) R. D. Shannon, *Acta Crystallogr., Sect. A: Cryst. Phys. Diffr., Theor. Gen. Crystallogr.*, 1976, **A32**, 751.
20 J. V. de Mello, H. F. Wittmann, R. H. Friend, *Adv. Mater.*, 1997, **9**, 230.
21 S. Marks, J. Heck, P. O. Burgos, C. Feldmann, P. W. Roesky, *J. Am. Chem. Soc.*, 2012, **134**, 16983.
22 J. C. Rybak, M. Hailmann, P. R. Matthes, A. Zurawski, J. Heck, C. Feldmann, S. Götzendörfer, J. Meinhardt, G. Sextl, H. Kohlmann, S. Sedlmaier, W. Schnick, K. Müller-Buschbaum, *J. Am. Chem. Soc.*, 2013, **135**, 6896.
23 Z. Hulvey, J. D. Furman, S. A. Turner, M. Tang, A. K. Cheetham, *Cryst. Growth Des.*, 2010, **10**, 2041.
24 Z. Wang, V. C. Kravtsov, R. B. Walsh, M. J. Zaworotko, *Cryst. Growth Des.*, 2007, **7**, 1154.
25 T.-H. Chen, I. Popov, O. Zenasni, O. Daugulis, O. Š. Miljanić, *Chem. Commun.*, 2013, **49**, 6846.
26 S. V. Larionov, L. I. Myachina, L. A. Glinskaya, I. V. Korol'kov, E. M. Uskov, O. V. Antonova, V. M. Karpov, V. E. Platanov, V. P. Fadeeva, *Russ. J. Coord. Chem.*, 2012, **38**, 717.
27 S. V. Larionov, L. I. Myachina, L. A. Sheludyakova, I. V. Korol'kov, O. V. Antonova, V. M. Karpov, V. E. Platanov, V. P. Fadeeva, *Russ. J. Gen. Chem.*, 2014, **84**, 1193.
28 E. A. Mikhalyova, S. V. Kolotilov, M. Zeller, L. K. Thompson, A. W. Addison, V. V. Pavlishchuk, A. D. Hunter, *Dalton Trans.*, 2011, **40**, 10989.

Table of contents entry

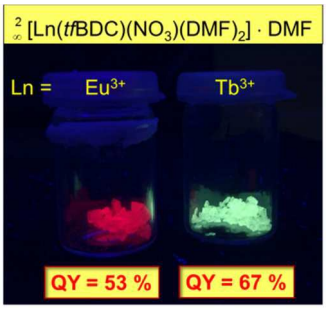

Ten lanthanide coordination polymers with tetrafluoroterephthalate as linker were synthesized. The Europium and Terbium compounds exhibit intense red and green emission in the visible with quantum yields up to 67 %.

Journal Name RSCPublishing

ARTICLE

Table 1. Details of X-ray Single Crystal Structure Analysis of compounds **1**-**5**.

Formula	$EuC_{17}H_{21}F_4N_4O_{10}$	$GdC_{17}H_{21}F_4N_4O_{10}$	$TbC_{17}H_{21}F_4N_4O_{10}$	$HoC_{17}H_{21}F_4N_4O_{10}$	$TmC_{17}H_{21}F_4N_4O_{10}$
Formula weight [g · mol^{-1}]	669.34	674.63	676.30	682.31	686.31
Crystal description	block, colorless	block, colorless	block, colorless	block, pink	block, colorless
Crystal size [mm]	0.50 x 0.20 x 0.20	0.60 x 0.50 x 0.30	0.40 x 0.25 x 0.15	0.30 x 0.25 x 0.20	0.70 x 0.50 x 0.30
Space group, Z	*C*2/*c* (no. 15), 8	*C*2/*c* (no. 15), 8	*C*2/*c* (no. 15), 8	*C*2/*c* (no. 15), 8	*C*2/*c* (no. 15), 8
a [pm]	2208.5(3)	2211.8(4)	2215.7(3)	2204.7(4)	2200.7(2)
b [pm]	1139.40(13)	1139.96(16)	1136.80(13)	1132.19(15)	1127.42(10)
c [pm]	2057.8(3)	2057.0(4)	2056.6(3)	2051.5(6)	2048.4(2)
β [deg]	111.243(11)	111.147(17)	111.047(11)	111.38(2)	111.459(8)
V [x 10^6 pm^3]	4826.3(11)	4837.2(15)	4834.6(11)	4768.4(18)	4730.0(8)
calc. density [g · cm^{-3}]	1.842	1.853	1.858	1.901	1.928
Absorption correction	numerical	numerical	numerical	numerical	numerical
Diffractometer (all Mo *Kα* radiation)	Stoe IPDS I	Stoe IPDS I	Stoe IPDS II	Stoe IPDS I	Stoe IPDS I
Temperature [K]	293(2)	293(2)	293(2)	293(2)	293(2)
$2\theta_{max}$ [deg]	56.2	56.2	54.6	56.4	54.4
Index ranges	-29 ≤ h ≤ 28 -14 ≤ k ≤ 14 -27 ≤ l ≤ 15	-29 ≤ h ≤ 28 -14 ≤ k ≤ 15 -27 ≤ l ≤ 25	-28 ≤ h ≤ 28 -14 ≤ k ≤ 14 -26 ≤ l ≤ 26	-28 ≤ h ≤ 29 -14 ≤ k ≤ 14 -27 ≤ l ≤ 27	-28 ≤ h ≤ 28 -14 ≤ k ≤ 14 -23 ≤ l ≤ 26
Reflections: measured / independent	9149 / 5224	10905 / 4124	11978 / 3977	10838 / 4073	17808 / 3914
Significant reflections	3597 with I > 2σ(I)	2085 with I > 2σ(I)	2827 with I > 2σ(I)	2616 with I > 2σ(I)	3493 with I > 2σ(I)
R(int)	0.032	0.152	0.088	0.102	0.089
Parameters / restraints	335 / 0	335 / 0	337 / 0	335 / 0	336 / 0
GooF = S_{all}	0.92	0.81	0.89	0.92	1.04
R[$F^2 > 2\sigma(F^2)$]	0.033	0.064	0.044	0.070	0.029
wR(F^2)	0.075	0.144	0.116	0.180	0.079
$\Delta\rho_{max}$ / $\Delta\rho_{min}$ [e x 10^{-6} pm^{-3}]	-1.38 / 1.08	-1.77 / 2.37	-0.83 / 0.85	-3.22 / 3.95	-1.41 / 1.40

Table 2. Details of X-ray Single Crystal Structure Analysis of compounds **6-10**.

Formula	$SmC_{16}H_{21}F_4N_6O_{12}$	$EuC_{16}H_{21}F_4N_6O_{12}$	$HoC_{12}H_{12}F_4NO_9S_2$	$ErC_{12}H_{12}F_4NO_9S_2$	$TmC_{12}H_{12}F_4NO_9S_2$
Formula weight [g · mol^{-1}]	715.74	717.35	619.28	621.61	623.28
Crystal description	block, yellow	block, colorless	block, pink	block, pink	block, colorless
Crystal size [mm]	0.30 x 0.30 x 0.20	0.30 x 0.20 x 0.20	0.20 x 0.10 x 0.10	0.45 x 0.30 x 0.25	0.40 x 0.20 x 0.10
Space group, Z	$P\bar{1}$, 2	$P\bar{1}$, 2	*Pbca*, 8	*Pbca*, 8	*Pbca*, 8
a [pm]	1098.16(13)	1094.65(5)	1546.09(17)	1541.77(13)	1535.08(4)
b [pm]	1116.45(13)	1111.55(5)	1505.99(15)	1504.82(9)	1496.76(4)
c [pm]	1152.91(12)	1146.84(5)	1670.57(15)	1667.49(11)	1657.58(6)
α [deg]	101.818(9)	101.707(3)	90	90	90
β [deg]	104.289(9)	104.300(3)	90	90	90
γ [deg]	101.705(9)	101.651(3)	90	90	90
V [x 10^6 pm^3]	1292.0(3)	1276.49(10)	3889.7(7)	3868.7(5)	3808.5(2)
calc. density [g · cm^{-3}]	1.840	1.866	2.115	2.134	2.174
Absorption correction	numerical	numerical	numerical	numerical	numerical
Diffractometer (all Mo *Kα* radiation)	Stoe IPDS II	Stoe IPDS II	Stoe IPDS II	Stoe IPDS II	Stoe IPDS II
Temperature [K]	293(2)	293(2)	293(2)	293(2)	293(2)
$2\theta_{max}$ [deg]	59.0	58.4	54.6	54.6	53.6
Index ranges	-15 ≤ h ≤ 15 -15 ≤ k ≤ 15 -15 ≤ l ≤ 15	-12 ≤ h ≤ 15 -15 ≤ k ≤ 15 -15 ≤ l ≤ 15	-19 ≤ h ≤ 19 -19 ≤ k ≤ 19 -21 ≤ l ≤ 21	-19 ≤ h ≤ 19 -19 ≤ k ≤ 18 -18 ≤ l ≤ 21	-19 ≤ h ≤ 19 -18 ≤ k ≤ 18 -20 ≤ l ≤ 20
Reflections: measured / independent	25552 / 7176	20469 / 6852	50858 / 4107	40534 / 4305	43741 / 3828
Significant reflections	5383 with I > 2σ(I)	6422 with I > 2σ(I)	2159 with I > 2σ(I)	3635 with I > 2σ(I)	2952 with I > 2σ(I)
R(int)	0.088	0.037	0.188	0.045	0.097
Parameters / restraints	353 / 0	353 / 0	266 / 0	267 / 0	266 / 0
GooF = S_{all}	1.08	1.07	0.90	1.11	1.03
R[$F^2 > 2\sigma(F^2)$]	0.046	0.023	0.047	0.035	0.028
wR(F^2)	0.086	0.060	0.075	0.101	0.069
$\Delta\rho_{max}$ / $\Delta\rho_{min}$ [e x 10^{-6} pm^{-3}]	-2.06 / 1.02	-0.86 / 0.74	-1.25 / 1.03	-1.67 / 1.17	-1.59 / 0.70

Table 3. Ionic Radii and Selected Interatomic Distances of Compounds **1**-**10**.

Ln^{3+} ion	corresponding compound	ionic radii[19] [pm]	Interatomic Distances [pm]		
			Ln^{3+} - Ln^{3+}	Ln^{3+} - O	$\Delta[(Ln^{III}\text{-}O)_{max}\text{-}(Ln^{III}\text{-}O)_{min}]$
Eu^{3+}	**1**	126.0 (CN = 9)	406.67(8)	238.7(4) – 262.3(3)	23.6
Gd^{3+}	**2**	124.7 (CN = 9)	404.6(2)	238.1(11) – 262.0(7)	23.9
Tb^{3+}	**3**	123.5(CN = 9)	402.84(8)	235.1(6) – 260.4(5)	25.3
Ho^{3+}	**4**	121.2 (CN = 9)	402.0(1)	233.1(8) – 261.9(9)	28.8
Tm^{3+}	**5**	119.2 (CN = 9)	399.98(5)	231.0(3) – 261.0(3)	30.0
Sm^{3+}	**6**	127.2 (CN = 9)	408.05(7)	236.8(3) – 260.1(3)	23.3
Eu^{3+}	**7**	126.0 (CN = 9)	405.85(3)	235.5(2) – 259.4(2)	23.9
Ho^{3+}	**8**	115.5 (CN = 8)	443.33(6)	229.4(6) – 244.2(7)	14.8
Er^{3+}	**9**	114.4 (CN = 8)	441.08(5)	229.0(4) – 243.6(4)	14.6
Tm^{3+}	**10**	113.4 (CN = 8)	439.48(5)	227.7(3) – 242.2(4)	14.5

Table 4. Known Crystal Structures of Coordination Polymers Containing Ln^{3+} Cations and $tfBDC^{2-}$ Linkers.

Type	General Composition	Referenz: Ln^{3+}	Space Group, Z	Coordination Number (CN)
I	$^{3}_{\infty}[Ln^{III}(tfBDC)_{3/2}(DMF)_{1/2}(H_2O)_{1/2}] \cdot$ ½ DMF	Ref. 7: Er^{3+}	$P\bar{1}$, 4	8
II	$^{2}_{\infty}[Ln^{III}(tfBDC)_{3/2}(DMF)] \cdot H_2O$	Ref. 27: Pr^{3+}, Nd^{3+}	*C*2, 4	9
III	$^{2}_{\infty}[Ln^{III}(tfBDC)_{3/2}(DEF)(EtOH)] \cdot DEF$	Ref. 12: La^{3+}, Nd^{3+}, Eu^{3+}, Gd^{3+}, Tb^{3+}	*C*2/*c*, 8	9
IV	$^{2}_{\infty}[Ln^{III}(tfBDC)(NO_3)(DMF)_2] \cdot DMF$	Ref. 11: Ce^{3+}, Pr^{3+}, Nd^{3+}, Sm^{3+}, Dy^{3+}, Er^{3+}, Yb^{3+} This work: Eu^{3+}, Gd^{3+}, Tb^{3+}, Ho^{3+}, Tm^{3+}	*C*2/*c*, 8	9
V	$^{2}_{\infty}[Ln^{III}(tfBDC)(NO_3)(DMSO)_2]$	This work: Ho^{3+}, Er^{3+}, Tm^{3+}	*Pbca*, 8	8
VI	$^{2}_{\infty}[Ln^{III}(tfBDC)(CH_3COO)(FA)_3] \cdot 3FA$	This work: Sm^{3+}, Eu^{3+}	$P\bar{1}$, 2	9
VII	$^{2}_{\infty}[Ln^{III}(tfBDC)_{3/2}(H_2O)_2] \cdot H_2O$	Ref. 25: Tb^{3+} Ref. 26: Sm^{3+}, Eu^{3+}, Dy^{3+}	*C*2, 4	9